ISSN 1063-7826, Semiconductors, 2017, Vol. 51, No. 2, pp. 232–238. © Pleiades Publishing, Ltd., 2017.
Original Russian Text © I.A. Prudaev, V.V. Kopyev, I.S. Romanov, V.L. Oleynik, 2017, published in Fizika i Tekhnika Poluprovodnikov, 2017, Vol. 51, No. 2, pp. 240–246.

PHYSICS OF SEMICONDUCTOR DEVICES

On the Effect of Ballistic Overflow on the Temperature Dependence of the Quantum Efficiency of InGaN/GaN Multiple Quantum Well Light-Emitting Diodes

I. A. Prudaev, V. V. Kopyev, I. S. Romanov, and V. L. Oleynik
National Research Tomsk State University, pr. Lenina 36, Tomsk, 634050 Russia
**e-mail: funcelab@gmail.com*
Submitted March 29, 2016; accepted for publication April 7, 2016

Abstract—The dependences of the quantum efficiency of InGaN/GaN multiple quantum well light-emitting diodes on the temperature and excitation level are studied. The experiment is performed for two luminescence excitation modes. A comparison of the results obtained during photo- and electroluminescence shows an additional (to the loss associated with Auger recombination) low-temperature loss in the high-density current region. This causes inversion of the temperature dependence of the quantum efficiency at temperatures lower than 220–300 K. Analysis shows that the loss is associated with electron leakage from the light-emitting-diode active region. The experimental data are explained using the ballistic-overflow model. The simulation results are in qualitative agreement with the experimental dependences of the quantum efficiency on temperature and current density.

DOI: 10.1134/S1063782617020166

1. INTRODUCTION

The temperature dependence of the external and internal quantum efficiency (QE) of InGaN/GaN multiple quantum well (MQW) light-emitting diodes was previously studied, e.g., in [1–16]. Two methods are most commonly used for studies: photoluminescence (PL) and electroluminescence (EL). The photoluminescence mode is convenient due to the fact that it allows the partial and in some cases complete exclusion of carrier leakage from quantum wells (QWs). For example, in the cryogenic temperature region where carrier leakage occurs by the tunneling mechanism, the lifetime appears much shorter than the tunneling time [17], which allows a conclusion concerning the complete absence of carrier leakage in the PL mode. At higher temperatures, the role of leakage can be stronger, if steady-state excitation conditions are not satisfied [18]. Nevertheless, carrier leakage during PL has a lower significance, since bipolar carrier generation occurs in the case at hand, in contrast to electroluminescence where the active region contains a larger number of electrons, i.e., high-mobility carriers.

It is possible that the temperature dependence of the QE for structures with InGaN/GaN QWs can be strictly described by taking into account the temperature dependence of the Shockley–Read nonradiative recombination (*A*), radiative (*B*), and Auger recombination (*C*) coefficients within the *ABC* model (see, e.g., that for the PL mode [1–4]), although there is still no consensus in this respect in publications [19, 20]. In the case of the *ABC* model, a decrease in the QE with temperature should be expected at all excitation levels, which is associated with an increase in the coefficients *A* and *C* [21]. Nevertheless, inversion of the temperature dependence of the QE was observed in some studies for the PL mode: the QE increases as the temperature increases to $T = 150$–220 K [5–7]. In the low-intensity region, where two competing processes associated with nonradiative (Shockley–Read) and radiative recombination take place, the QE reaches relatively high values (up to ~250% according to [7]). In the region of high pump powers, where the Auger recombination rate becomes significant, the increase in the QE with T is relatively low (to ~15% according to [6]). In both cases, inversion of the temperature dependence of the QE is explained by carrier delocalization from nonradiative recombination centers with increasing temperature [5–7].

In the electroluminescence mode, inversion of the temperature dependence of the QE can cause a stronger increase in the quantum efficiency with T (a 1.5–30-fold increase in the region of high current densities, $j > (1–10)$ A/cm^2 [8–14]). To explain this effect, tunneling leakage [8], a high injection level of electrons to the *p*-type region [9, 10], carrier escape from QWs [11], recombination-center activation with increasing carrier concentration [22], and ballistic electron transport [12, 13] have been considered in various studies.

Furthermore, possible causes of the inversion of the temperature dependence of the QE for high current densities, associated with a change in coefficient B with decreasing T due to a change in the density of states in the valence band [20]. It should also be noted that an increase in the QE with decreasing T can be observed in the case of light-emitting-diode heating or current crowding effects [20, 23], if the measurement conditions or experimental sample configuration are chosen incorrectly. A comprehensive analysis of the possible causes of inversion of the temperature dependence of the QE should be performed taking into account particular experimental conditions and sample structures.

In this paper, we present the experimental results of studying the temperature dependence of the QE in two modes (PL and EL). The dependences of the QE on j and T are analyzed using one of the possible models, i.e., the ballistic carrier overflow model. This model was proposed previously and used to explain the complex shape of the current–voltage (I–V) characteristics of InGaN/GaN MQW light-emitting diodes [13].

2. EXPERIMENTAL

A commercial blue light-emitting-diode structure grown by metal-organic chemical vapor deposition on a profiled Al_2O_3 (0001) substrate was used in the experiment. The density of threading dislocations, determined by etch pits, did not exceed 10^8 cm^{-2}. The total thickness of the active region of the structures was ~200 nm and included a buffer layer, multiple quantum wells, and a p-$Al_{0.15}Ga_{0.85}N$ barrier layer 30 nm thick. The period of n-$In_{0.15}Ga_{0.85}N$/GaN MQWs was ~17.5 nm; according to photoconductivity measurements, under resonant excitation (405 nm) the active region contains a total of 7 QWs. The p-layer thickness determined by atomic emission spectroscopy was ~280 nm. These structures were used to fabricate light-emitting diodes by planar technology with interdigital Ni/Au ohmic contacts (the contact resistance measured by the transmission line method (TLM) did not exceed 10^{-2} Ω cm^2). The light-emitting-diode area was 1 mm^2.

The dependences of the external quantum efficiency on the flowing current density (for EL) and excitation intensities (for PL) were measured in the experiment in a wide temperature range (T = 10–300 K). The maximum quantity efficiency taken as unity was observed at the lowest temperatures.

A cryogenic system based on a Janis CCS-300S/204 HT cryostat was used in the study. For a current density of $j < 3$ A/cm^2, measurements were performed under steady-state conditions using a Keithley 2636 source meter. In the pulsed mode, measurements were performed to $j = 200$ A/cm^2 at frequencies of 50 and 100 Hz (duration is 0.04×10^{-3} s) using a LeCroy104Xs oscilloscope. The QE was studied in the PL mode using an YAG laser with an average power of 22.4×10^{-3} W (duration is 10 ns, frequency is 0.2–1 kHz, and wavelength is 355 nm). The intensity of the focused excitation radiation was varied using glass attenuators with an ITO (indium–tin oxide) coating. The luminescence spectra and total radiation intensity were measured using a calibrated silicon photodetector and a USB 2000 (Ocean Optics) fiber-optic spectrometer.

The light-emitting-diode overheating was excluded by a high duty ratio of measurements in the pulsed mode and the use of a bulk copper holder of the light-emitting-diode crystal (~15 × 10 × 2 mm in size) which was pressed by a screw to a cold cryostat finger. The lack of overheating was judged by the short-wavelength luminescence shift characteristic of InGaN/GaN structures [1]. The absence of the current crowding effect was judged by the shape of the forward I–V characteristic in which a sharp increase in the current with increasing voltage is observed for the “efficiency droop” region [12, 13]. It was believed that current crowding should lead to the reverse effect, i.e., an increase in the sample resistance.

3. EXPERIMENTAL RESULTS

The experimental temperature dependences of the QE η, measured under various conditions are shown in Fig. 1. At low excitation intensities in the PL mode, a decrease in the quantum efficiency with T is observed, which is consistent with the results of other studies [1–3]. In this case, the temperature dependence of the QE is caused by the temperature dependence of the radiative and Shockley–Read recombination lifetimes. Within the ABC model, the quantum efficiency for this low excitation level is defined by the ratio of nonradiative- and radiative-recombination coefficients.

It follows from Fig. 1 that a slight temperature dependence of the quantum efficiency is observed for the PL mode at high excitation levels. A similar result was obtained previously in some studies for the PL and EL modes [1, 3, 15]. If we take into account that the decrease in the quantum efficiency, observed in this region, is associated with the Auger process, this points to the slight dependence of C on T.

The results of studying the quantum efficiency in the EL mode is also in qualitative agreement with the results of many studies [8–14]. In the low current density region, a temperature increase results in a decrease in the QE, which can also be caused by the ratio of the coefficients A and B. In the high current density region, strong inversion of the temperature dependence of the QE takes place; as T increases, the quantum efficiency increases by more than an order of magnitude.

It should be noted that the inversion of the temperature dependence of the quantum efficiency for the

EL mode is not always observed in the experiments [20]. For example, a decrease in the QE with increasing temperature at a high current density was observed in [15, 16], which is analogous to the PL mode in the case at hand. A possible explanation for this disagreement is given at the end of the following section within the presented ballistic-overflow model.

4. RESULTS AND DISCUSSION

4.1. Low-Temperature Loss

The qualitative difference of the temperature dependence of the QE in the high injection level region for two modes suggests that an additional loss mechanism (additional to the loss associated with Auger recombination) appears in the EL mode at low temperatures. In this case, the losses under consideration cannot be related to the temperature dependence of the recombination coefficients [20] or the activation of recombination centers with shorter lifetimes with increasing carrier concentration [22] (this is indicated by a comparison of the results of measurements of quantum efficiencies during PL and EL). The most obvious process responsible for losses is carrier leakage from the active region at high current densities. In this case, the leakage of electrons to the *p*-type region is most probable, since they have a smaller effective mass and relatively uniformly populate all quantum wells [24, 25]. Holes are mostly localized in the region of the first QWs (on the *p*-type layer side). This is especially true for low temperatures, when hole injection from localized acceptor states takes place [12, 26].

The application of concepts of a quasi-equilibrium system state, underlying the diffusion-drift model of charge transfer in structures with InGaN/GaN QWs [27, 28], does not allow explanation of the inversion of the temperature dependence of the QE due to leakage. This is mainly due to an exponential decrease in the probability of the thermal escape of electrons from quantum wells with decreasing temperature. This is indirectly confirmed by the results of [29] in which the compositional inhomogeneity of InGaN layers was considered in the three-dimensional simulation of carrier transport in the diffusion-drift approximation. It was shown that this model is valid for close-to-room temperatures; in the low-temperature region, the calculated and experimental data disagree.

In our opinion, electron tunneling to the *p*-type region over defect states from the active region or ballistic electron transport over QWs should be considered among the possible low-temperature leakage mechanisms. In the present paper, we consider the latter mechanism. Nevertheless, we also did not find any published data on simulation of the temperature inversion of the QE taking into account tunneling leakage.

Ballistic transport is characterized by the carrier relaxation time; the most probable mechanism of energy dissipation in GaN is the interaction with optical phonons [23]. In the case of elastic dissipation, the relaxation time, as the electron mean free path, increases with decreasing temperature [30], which should lead to an increase in the ballistic overflow. At the same time, it is known that the MQW-region resistance increases with decreasing temperature [31, 32]. Then the voltage drop at the MQW region will also increase with decreasing T for identical current densities. As a result, the potential energy of electrons injected from the *n*-type region should increase due to the voltage applied to the MQW region.

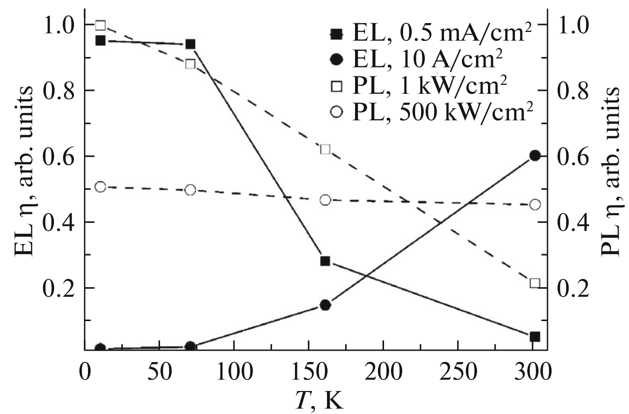

Fig. 1. Temperature dependence of the quantum efficiency η of the InGaN/GaN MQW light-emitting diode upon photo- (PL) and electroluminescence (EL) for various excitation levels.

4.2. Model Description

To calculate the dependences of the QE on j and T, we use the previously proposed phenomenological model [13]. In this model, the MQW region is divided into two parts: the space-charge-limited current (SCLC) region and the space-charge region (SCR) of the electron–hole transition. To describe the model, Fig. 2 schematically shows the energy diagram of the active region of a light-emitting diode with 7 QWs (a) at equilibrium and (b) under forward bias V. It is assumed that a temperature decrease leads to an increase in the role of the tunneling MQW conductance component, when carriers from one quantum well transfer to another via hopping transport (defect-assisted tunneling). Due to the density-of-states tail existing in the band gap of GaN barriers, charge is mostly transferred to some transport level whose position depends on temperature. The charge-transfer model previously proposed for amorphous semiconductors is adopted in this sense [33]. It is also taken into account that the localized states of quantum wells can manifest themselves as shallow electron traps. We previously showed that the application of this approach allows the description of experimental $I–V$ characteristics in the low-temperature region to the threshold current density corresponding to the begin-

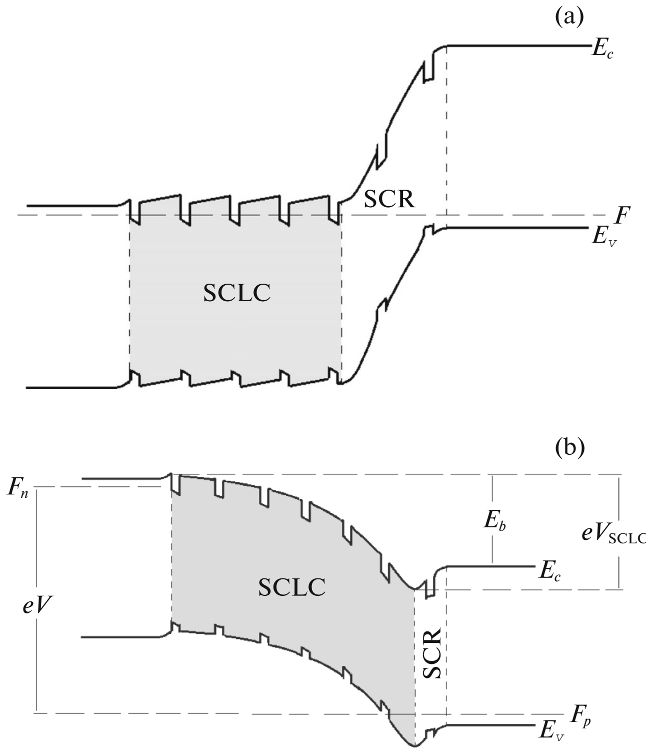

Fig. 2. Energy diagram of the InGaN/GaN MQW light-emitting diode (a) at equilibrium and (b) under forward bias V. E_c and E_v are the conduction- and valence-band edges, F is the Fermi level, F_n and F_p are the quasi-Fermi levels for electrons and holes.

ning of the QE droop region [13]. In this case, the space-charge-limited current density trapped at shallow traps obeys the expression [13]

$$j_t = [r(T)]^{-2} V_{\mathrm{SCLC}}^2, \tag{1}$$

where V_{SCLC} is the voltage at the charge-accumulation region in the MQWs and $r(T)$ is the empirical coefficient determined from the experimental I–V characteristics.

Here it should be specified that the current limiting mechanism in the MQW region can be of a different nature. Nevertheless, empirical formula (1) remains valid and can be used in simulation.

Upon achieving a forward voltage at the light-emitting diode, electrons injected from the n-type region gain the additional energy E_b, which results in an increase in the ballistic-conductance component over the entire MQW region (Fig. 2b). The ballistic-overflow current density is calculated according to the following expression [13]

$$j_b(V_b) = e\int_0^\infty f(E,T)N(E,T)\exp\left[-\frac{W}{\tau_{sc}v(E+eV_b,T)}\right] \times v(E+eV_b,T)dE, \tag{2}$$

where e is the elementary charge, $V_b = E_b/e$, W is the light-emitting diode active-region thickness, E is the electron energy relative to the conduction-band bottom, f is the Fermi–Dirac function, N is the density of quantum states in the conduction band, v is the electron velocity, and τ_{sc} is the relaxation time for electrons.

To take into account the different recombination mechanisms, the recombination current density j_R is calculated by the expression

$$j_R(V_{p-n}) = j_{\mathrm{nrad}} + j_{\mathrm{rad}} = ed\left[An_i\exp\left(\frac{eV_{p-n}}{2kT}\right) + Cn_i^3\exp\left(\frac{3eV_{p-n}}{2kT}\right) + Bn_i^2\exp\left(\frac{eV_{p-n}}{2kT}\right)\right], \tag{3}$$

where d is the quantum-well width (it is assumed that carrier recombination occurs only in the first quantum well from the p-region side at low temperatures [12, 13]), n_i is the intrinsic carrier concentration, and V_{p-n} is the voltage applied to the space-charge region of the electron–hole transition.

Analytical expression (3) is simplified and was obtained from the general definition of the recombination current without regard to the diffusion-drift redistribution of carriers within the active region (the current is limited only by recombination in one QW). The scheme of deriving the recombination current density for linear and quadratic cases is given in [34]; similarly, the dependence of the recombination current $j = j(V_{p-n})$ for cubic recombination is derived. The use of expression (3) allows the conclusions of the *ABC* model to be taken into account in calculating the dependences of QE on j and T.

Thus, the model under consideration is based on solution of the system of equations (1)–(3) for the equivalent circuit of the active region of the light-emitting diode, shown in Fig. 3. The dependences of the QE on j and T is simulated using the expression

$$\eta(j) = j_{\mathrm{rad}}/j_{\mathrm{total}}, \tag{4}$$

where j_{total} is the total current density over the entire structure, being the sum of expressions (1) and (2). The MQW voltage is calculated according to the expression $V = V_{\mathrm{SCLS}} + V_{p-n}$.

4.3. Simulation Results

The described model contains many unknown parameters, mainly A, B, C, and τ_{sc}. These parameters should depend on temperature and be controlled to some extent by the configuration and fabrication technology of the experimental samples. Measurements of their temperature dependences is difficult; therefore, at this stage of the study, only a qualitative analysis using published data on A, B, C, and τ_{sc} seems possible.

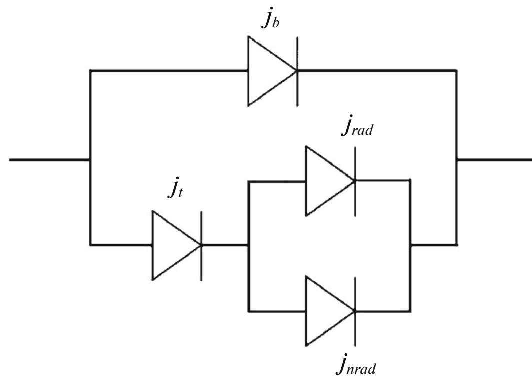

Fig. 3. Equivalent circuit of the active region of the InGaN/GaN MQW light-emitting diode, used in the simulation.

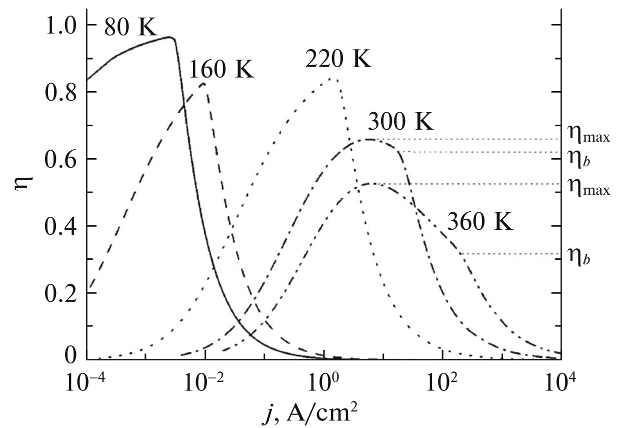

Fig. 4. Dependences of the quantum efficiency of electroluminescence of the InGaN/GaN MQW light-emitting diode, calculated for various temperatures (the radiation-emission coefficient was set to unity).

The following parameters were used in the calculation as temperature-independent ones: $C = 10^{-30}$ cm^6/s [19], $\tau_{sc} = 9 \times 10^{-15}$ s [23], $d = 2$ nm, and $W = 100$ nm. Although the Auger-recombination coefficient should increase with temperature due to an increase in the thermal velocity of carriers, according to experimental data, the dependence $C(T)$ is weak, which was mentioned in section 3. At the same time, the parameter τ_{sc} can increase with decreasing temperature [30]. Nevertheless, the use of accurate dependences of C and τ_{sc} on T should not affect the qualitative shape of the dependence of the quantum efficiency on T and j, and an increase in τ_{sc} with decreasing T should enhance the electron leakage process at low temperatures.

The parameters depending on T are listed in the table. The values of $r(T)$ were obtained by approximating the experimental $I–V$ characteristic of the light-emitting diode, taking into account expression (1) by the technique described in [13, 32]. The values of the coefficients A and B for room temperature were taken from [19]. The temperature dependences of the recombination coefficients were chosen from general concepts that the lifetime relative to nonradiative recombination increases with decreasing temperature, while the lifetime relative to radiative recombination decreases [21]. The order of magnitude of changes in A and B with decreasing temperature was chosen according to the data of [22], which made it possible to achieve qualitative agreement between the calculated and experimental dependences $\eta(T, j)$ for the region of low current densities.

The simulation results are shown in Figs. 4 and 5. It follows from Fig. 4 that the temperature increase results in a shift of the dependence $\eta(j)$ to high current densities, which is in qualitative agreement with different experimental data [8, 9, 11–14]. As a result, inversion of the temperature dependence of the quantum efficiency appears in the region of high current densities (Fig. 5).

As shown in Fig. 4, the dependence of the QE on j in the efficiency droop region qualitatively changes as T increases from 220 to 300 K. At low temperatures ($T \leq 220$ K), the QE sharply decreases with increasing j due to an increase in the ballistic overflow or, what is the same, an increase in the ratio j_b/j_R. At high temperatures ($T \geq 300$ K), the QE droop region can be divided into two parts. The first one corresponds to a relatively slight decrease in the QE with increasing j (interval $\eta_b < \eta < \eta_{max}$ shown in Fig. 4). An analysis of the model shows that this range is associated with the effect of the Auger-recombination process. The second part is characterized by a sharp decrease in the QE (interval $0 < \eta < \eta_b$ shown in Fig. 4). In this case, the nature of the QE decrease is the same as at $T \leq 220$ K.

Thus, it follows from the simulation results that Auger recombination has the greatest effect on the QE droop with increasing j for close-to-room temperatures (and above). At lower temperatures, the ballistic electron overflow to the p-type region has the most significant effect on the QE droop.

Parameters used in simulation of the dependence of the quantum efficiency on T and j

Temperature, K	80	160	220	300	360
A, s^{-1}	0.3×10^6	2×10^6	8×10^6	1.5×10^7	2×10^7
B, cm^3 s^{-1}	5×10^{-10}	2×10^{-10}	4×10^{-11}	1.5×10^{-11}	1×10^{-11}
r, B/A$^{1/2}$	106	64	5	1.5	0.5

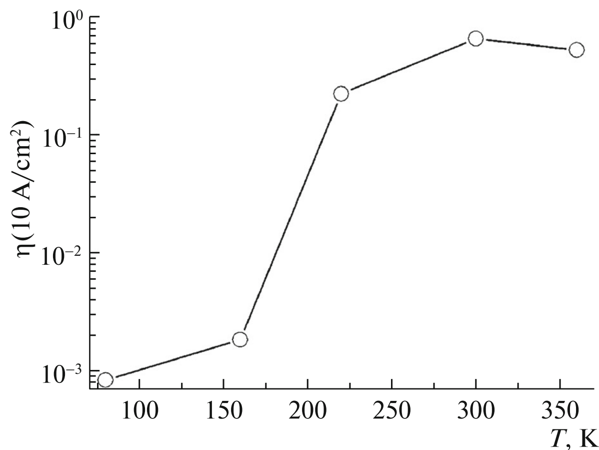

Fig. 5. Calculated temperature dependence of the quantum efficiency of electroluminescence of the InGaN/GaN MQW light-emitting diode for the current density j = 10 A/cm^2.

Additional calculations showed that the role of ballistic overflow decreases with decreasing voltage drop at the MQW region. Formally, this means that the lower parameter r, the higher the values of j corresponding to the beginning of ballistic overflow. In the limit, at $r = 0$, the described model completely transforms to the *ABC* model, when the inversion of the temperature dependence of the QE in the region of high j is lacking. In this case, no current limitations are observed in the I–V characteristic, except for ohmic losses on the series resistance of contacts and passive regions of the light-emitting diode. From this standpoint, the explanation of the results of many studies in which the experimental dependences $\eta(T, j)$ are described by the *ABC* model becomes clear. It is possible that the *ABC* model is applicable to light-emitting diodes whose active region contains a small number of QWs, a superlattice (a set of QWs separated by thin barriers) or do not contain additional buffer layers from the n-type layer side, which lead to current limitation at low temperatures. In such light-emitting diodes, the active-region resistance is low due to the uniform spreading of holes and electrons over all structure layers. However, an analysis from this standpoint is complicated for already published data. This is because most studies were performed previously on commercial light-emitting diodes [8, 9, 11, 15, 16], whose active-region structure features are not described in detail.

5. CONCLUSIONS

Various cases of experimental observations of inversion of the temperature dependence of the quantum efficiency in the photo- and electroluminescence modes were considered. Of most practical interest is the electroluminescence mode in the region of high current densities ($j > 1$–10 A/cm^2). It was shown that inversion of the temperature dependence of the quantum efficiency can be observed at high current densities, when the quantum efficiency sharply increases with temperature. To explain this effect, the ballistic-overflow model was used, which takes into account an increase in the resistance of the region of multiple quantum wells with decreasing temperature. An analysis of the simulation results showed that the decrease in the quantum efficiency in the low-temperature region is caused by ballistic electron overflow to the p-type region, while the decrease at temperatures above room temperature is also associated with Auger recombination. Therefore, the quantum efficiency increases with temperature at $T < 220$–300 K. The model under consideration allows qualitative explanation of the experimental results, and its basic assumptions can be used when constructing a more rigorous theory of carrier transport in structures with multiple InGaN/GaN quantum wells.

ACKNOWLEDGMENTS

This study was supported by the Ministry of Education and Science of Russia (State contract no. 3.1206.2014) and the program of increasing the international competitiveness of Tomsk State University for 2013–2020.

REFERENCES

1. S. Watanabe, N. Yamada, M. Nagashima, Y. Ueki, C. Sasaki, Y. Yamada, T. Taguchi, K. Tadatomo, H. Okagawa, and H. Kudo, Appl. Phys. Lett. **83**, 4906 (2003).
2. A. Sasaki, S. Shibakawa, Y. Kawakami, K. Nishizuka, Y. Narukawa, and T. Mukai, Jpn. J. Appl. Phys. **45**, 8719 (2006).
3. T. Kohno, Y. Sudo, M. Yamauchi, K. Mitsui, H. Kudo, H. Okagawa, and Y. Yamada, Jpn. J. Appl. Phys. **51**, 072102 (2012).
4. Y. C. Shen, G. O. Mueller, S. Watanabe, N. F. Gardner, A. Munkholm, and M. R. Krames, Appl. Phys. Lett. **91**, 141101 (2007).
5. J. H. Chen, Z. C. Feng, J. C. Wang, H. L. Tsai, J. R. Yang, A. Parekh, E. Armour, and P. Faniano, J. Cryst. Growth **287**, 354 (2006).
6. I. A. Prudaev, I. S. Romanov, V. V. Kop'ev, S. B. Shirapov, O. P. Tolbanov, and S. S. Khludkov, Russ. Phys. J. **56**, 757 (2013).
7. J. Ma, X. Ji, G. Wang, X. Wei, H. Lu, X. Yi, R. Duan, J. Wang, Y. Zeng, J. Li, F. Yang, C. Wang, and G. Zou, Appl. Phys. Lett. **101**, 131101 (2012).
8. N. I. Bochkareva, E. A. Zhirnov, A. A. Efremov, E. T. Rebane, R. I. Gorbunov, and Yu. G. Shreter, Semiconductors **39**, 594 (2005).
9. D. S. Meyaard, G.-B. Lin, Q. Shan, J. Cho, E. F. Schubert, H. Shim, M.-H. Kim, and C. Sone, Appl. Phys. Lett. **99**, 251115 (2011).

10. A. S. Pavluchenko, I. V. Rozhansky, and D. A. Zakheim, Semiconductors **43**, 1351 (2009).
11. K. Fudjiwara, H. Jimi, and K. Kaneda, Phys. Status Solidi C **6**, S814 (2009).
12. I. A. Prudaev, I. Yu. Golygin, S. B. Shirapov, I. S. Romanov, S. S. Khludkov, and O. P. Tolbanov, Semiconductors **47**, 1382 (2013).
13. I. Prudaev, O. Tolbanov, and S. Khludkov, Phys. Status Solidi A **212**, 930 (2015).
14. C. H. Wang, J. R. Chen, C. H. Chiu, H. C. Kuo, Y.-L. Li, T. C. Lu, and S. C. Wang, IEEE Photon. Tech. Lett. **22**, 236 (2010).
15. I. E. Titkov, S. Yu. Karpov, A. Yadav, V. L. Zerova, M. Zulonas, B. Galler, M. Strassburg, I. Pietzonka, H.-J. Lugauer, and E. U. Rafailov, IEEE J. Quantum Electron. **50**, 911 (2014).
16. A. Laubsch, M. Sabathil, W. Bergbauer, M. Strassburg, H. Lugauer, M. Peter, S. Lutgen, N. Linder, K. Streubel, J. Hader, J. V. Moloney, B. Pasenow, and S. W. Koch, Phys. Status Solidi C **6**, S913 (2009).
17. V. S. Sizov, V. V. Neplokh, A. F. Tsatsulnikov, A. V. Sakharov, V. V. Lundin, E. E. Zavarin, A. E. Nikolaev, A. M. Mintairov, and J. L. Merz, Semiconductors **44**, 1567 (2010).
18. M. F. Schubert, J. Xu, Q. Dai, F. W. Mont, J. K. Kim, and E. F. Schubert, Appl. Phys. Lett. **94**, 081114 (2009).
19. J. Piprek, Phys. Status Solidi A **207**, 2217 (2010).
20. S. Yu. Karpov, Opt. Quantum Electron. **47**, 1293 (2015).
21. F. E. Shubert, *Light Emitting Diodes* (Fizmatlit, Moscow, 2008; Cambridge Univ. Press, Cambridge, 2006), Chap. 2, rus. p. 60.
22. J. Hader, J. V. Moloney, and S. W. Koch, Appl. Phys. Lett. **99**, 181127 (2011).
23. X. Ni, X. Li, J. Lee, S. Liu, V. Avrutin, A. Matulionis, U. Ozgur, and H. Morkoc, Superlatt. Microstruct. **48**, 133 (2010).
24. A. V. Sakharov, V. V. Lundin, E. E. Zavarin, M. A. Sinitsyn, A. E. Nikolaev, S. O. Usov, V. S. Sizov, G. A. Mikhailovsky, N. A. Cherkashin, M. Hytch, F. Hue, E. V. Yakovlev, A. V. Lobanova, and A. F. Tsatsul'nikov, Semiconductors **43**, 812 (2009).
25. D. A. Zakheim, A. S. Pavluchenko, D. A. Bauman, K. A. Bulashevich, O. V. Khokhlev, and S. Yu. Karpov, Phys. Status Solidi A **209**, 456 (2012).
26. D. Yang, L. Wang, W.-B. Lv, Z.-B. Hao, and Y. Luo, Superlatt. Microstruct. **82**, 26 (2015).
27. K. A. Bulashevich, V. F. Mymrin, S. Yu. Karpov, I. A. Zhmakin, and A. I. Zhmakin, J. Comp. Phys. **213**, 214 (2006).
28. S. Yu. Karpov, Proc. SPIE **7939**, 79391C (2011).
29. D. A. Browne, B. Mazumder, Y.-R. Wu, and J. S. Speck, J. Appl. Phys. **117**, 185703 (2015).
30. A. I. Anselm, *Introduction to Semiconductor Theory* (Prentice-Hall, Englewood Cliffs, 1981; Nauka, Moscow, 1978), Chap. 8, par. 6, rus. p. 484.
31. I. A. Prudaev, I. V. Ivonin, and O. P. Tolbanov, Russ. Phys. J. **54**, 1372 (2012).
32. I. A. Prudaev, Yu. L. Zubrilkina, A. A. Baktybaev, and I. S. Romanov, Russ. Phys. J. **57**, 1246 (2015).
33. D. Monroe, Phys. Rev. Lett. **54**, 146 (1985).
34. P. G. Eliseev, *Introduction to the Physics of Injection Lasers* (Nauka, Moscow, 1983), Chap. 6, p. 186 [in Russian].

Translated by A. Kazantsev